


Searching for the light leptophilic gauge boson Z_x via four-lepton final states at the CEPC*

Chong-Xing Yue (岳崇兴)^{1,2†} Yan-Yu Li (李妍钰)^{1,2‡} 
 Mei-Shu-Yu Wang (王美舒羽)^{1,2§} Xin-Meng Zhang (张欣蒙)^{1,2‡}

¹Department of Physics, Liaoning Normal University, Dalian 116029, China

²Center for Theoretical and Experimental High Energy Physics, Liaoning Normal University, Dalian 116029, China

Abstract: We investigate the possibility of detecting the leptophilic gauge boson Z_x predicted by the $U(1)_{L_e-L_\mu}$ model via the processes $e^+e^- \rightarrow \ell^+\ell^-Z_x(Z_x \rightarrow \ell^+\ell^-)$ and $e^+e^- \rightarrow \ell^+\ell^-Z_x(Z_x \rightarrow \nu_\ell\bar{\nu}_\ell)$ at the Circular Electron Positron Collider (CEPC) with a center of mass energy $\sqrt{s} = 240$ GeV and luminosity $\mathcal{L} = 5.6$ ab⁻¹. We provide the expected sensitivities of the CEPC to the parameter space at the 1σ , 2σ , 3σ , and 5σ levels.

Keywords: light gauge boson Z_x , $U(1)_{L_e-L_\mu}$ model, Circular Electron Positron Collider

DOI: 10.1088/1674-1137/ad25f5

I. INTRODUCTION

The Circular Electron Positron Collider (CEPC) [1] is a particle physics research program of great scientific significance and has great potential. The concept of the CEPC is developed in the context of many international large colliders, such as the Large Hadron Collider (LHC) at the European Center for Nuclear Research (CERN). In contrast to previous colliders with high energy consumption and costs as well as the pressure of data processing and storage, the CEPC has unique features and advantages. Firstly, the CEPC is an electron collider in which positrons and electrons collide with each other to produce high-energy particle events. Unlike hadron collisions, electron collisions produce particle events that are much clearer and more controllable, facilitating precise measurements and particle identification. Secondly, the CEPC plans to build a highly detailed detector that will be able to capture and record all the important information in particle collisions, providing physicists with a large amount of data to study the behavior of elementary particles. In addition, the CEPC will invest significant effort in improving data processing and storage techniques to cope with the high density of collision data. Finally, the CEPC has a much brighter and cleaner experimental environment. The standard model (SM) observables can

be studied with unprecedented precision, and the precision of many electroweak observables can be improved by an order of magnitude or more. Therefore, the CEPC offers an unmatched opportunity for precision measurements and searches far beyond the standard model (BSM) physics.

Among the many new physics (NP) scenarios, a class of models can predict the existence of leptophilic gauge boson Z_x ; this kind of new neutral gauge boson arises due to the extension of a group in the standard model (SM) with the $U(1)_{L_x-L_y}$ for $x, y \in \{e, \mu, \tau\}$ [2–4]. The global symmetry $U(1)_{L_x-L_y}$ can be introduced to the SM, which is anomaly-free, without any additional particles [5, 6]. When the $U(1)_{L_x-L_y}$ gauge symmetry is spontaneously broken, the leptophilic gauge boson Z_x gains mass. This class of models can be a good solution to solve some problems in the SM, such as the neutrino mass and mixing problem [7–9], the dark matter dark energy problem [9–12], and the muon anomalous magnetic moment problem [13–15]. In our paper, we discuss the possibility of probing this class of the leptophilic gauge boson Z_x at the CEPC.

The study of the leptophilic gauge boson Z_x is an important step in exploring NP. The Z_x boson can be produced at current collider experiments. For example, at the LHC, the leptophilic gauge boson Z_x is mainly produced

Received 5 December 2023; Accepted 2 February 2024; Published online 3 February 2024

* Supported by the National Natural Science Foundation of China (11875157, 12147214)

† E-mail: cxyue@lnnu.edu.cn

‡ E-mail: lyy3390@163.com

§ E-mail: 1404592974@qq.com

‡ E-mail: 398443768@qq.com



Content from this work may be used under the terms of the Creative Commons Attribution 3.0 licence. Any further distribution of this work must maintain attribution to the author(s) and the title of the work, journal citation and DOI. Article funded by SCOAP³ and published under licence by Chinese Physical Society and the Institute of High Energy Physics of the Chinese Academy of Sciences and the Institute of Modern Physics of the Chinese Academy of Sciences and IOP Publishing Ltd

via the Drell-Yan process, where the Z_x is radiated from the final-state leptons; the constraints on the Z_x boson can be given via the processes $pp \rightarrow 4\ell, 3\ell + E_T^{\text{miss}}, 2\ell + E_T^{\text{miss}}$, or $1\ell + E_T^{\text{miss}}$ [16–19]. At the KEKB collider, the leptophilic gauge boson Z_x is produced via the process $e^+e^- \rightarrow \mu^+\mu^-Z_x (Z_x \rightarrow \mu^+\mu^-)$ in the framework of the $U(1)_{L_\mu-L_\tau}$ model in the small mass range $M_{Z_x} < 10$ GeV [20]. The processes $e^+e^- \rightarrow Z_x \rightarrow \ell^+\ell^-$ or $q\bar{q}$ [21] and $e^+e^- \rightarrow \gamma Z_x (\rightarrow \ell^+\ell^-, \mu^+\mu^-)$ [22] can also be used to search for the Z_x boson at the LEP and BABAR. Most of the LHC (and Tevatron) bounds coming from resonance searches do not directly apply to such a neutral leptophilic sector. The relevant collider constraints of the $U(1)_{L_e-L_\mu}$ model mainly come from the LEP and are generally much weaker than the direct LHC constraints applicable for hadrophilic resonances [23]. Therefore, the future e^+e^- colliders are uniquely capable of probing the leptophilic gauge boson Z_x to unprecedented mass and coupling values. Previous studies [24, 25] have investigated the sensitivity of the process $e^+e^- \rightarrow Z_x\gamma$ to explore the leptophilic gauge boson Z_x in future e^+e^- colliders. In general, properties of any new particle can be studied via different processes, even for the same collider experiments. Furthermore, we find that there are few studies that search for the gauge boson Z_x predicted by the $U(1)_{L_e-L_\mu}$ model via four-lepton final state processes at future e^+e^- colliders; hence, we propose searching for this kind of leptophilic gauge boson Z_x via the processes $e^+e^- \rightarrow \ell^+\ell^-Z_x (Z_x \rightarrow \ell^+\ell^-)$ and $e^+e^- \rightarrow \ell^+\ell^-Z_x (Z_x \rightarrow \nu_\ell\bar{\nu}_\ell)$ at the 240 GeV CEPC. We expect these processes to give better sensitivities in the certain mass range.

The remainder of the paper is organized as follows. Section II briefly introduces the $U(1)_{L_e-L_\mu}$ model and summarizes the constraints of existing experiments on the model. Based on the details of the analysis of the Z_x signal processes $e^+e^- \rightarrow \ell^+\ell^-Z_x (Z_x \rightarrow \ell^+\ell^-)$ and $e^+e^- \rightarrow \ell^+\ell^-Z_x (Z_x \rightarrow \nu_\ell\bar{\nu}_\ell)$ and the relevant SM backgrounds, the sensitivity projections of the CEPC to the $U(1)_{L_e-L_\mu}$ model parameter space are presented and compared with other experimental results in Section III. Finally, the conclusion and discussion are given in Section IV.

II. THE $U(1)_{L_e-L_\mu}$ MODEL

The $U(1)_{L_x-L_y}$ model [2–4] comprises the SM gauge group $SU(3)_C \otimes SU(2)_L \otimes U(1)_Y$ expanding a $U(1)_{L_x-L_y}$ group without introducing an anomaly. This surprising feature is the main motivation considered here. For convenience, in Table 1, we list the lepton charges for the $U(1)_{L_x-L_y}$ models. Here, e , μ , and τ are three generations of charged leptons; ν_e , ν_μ , and ν_τ represent the corresponding left-handed neutrinos, respectively.

The Lagrangian part of the $U(1)_{L_e-L_\mu}$ model can be written as

Table 1. Lepton charges corresponding to the $U(1)_{L_x-L_y}$ models.

Model	Charge		
	e, ν_e	μ, ν_μ	τ, ν_τ
$L_e - L_\mu$	1	-1	0
$L_e - L_\tau$	1	0	-1
$L_\mu - L_\tau$	0	$L_e - \frac{1}{2}(L_\mu + L_\tau)$	-1
$L_e - \frac{1}{2}(L_\mu + L_\tau)$	1	$-\frac{1}{2}$	$\frac{1}{2}$
$L_e + 2(L_\mu + L_\tau)$	1	2	2

$$\begin{aligned} \mathcal{L}(Z_x) = & -g'Z_x^\alpha [Q_e(\bar{e}\gamma_\alpha e + \bar{\nu}_e\gamma_\alpha P_L\nu_e) + Q_\mu(\bar{\mu}\gamma_\alpha\mu + \bar{\nu}_\mu\gamma_\alpha P_L\nu_\mu) \\ & + Q_\tau(\bar{\tau}\gamma_\alpha\tau + \bar{\nu}_\tau\gamma_\alpha P_L\nu_\tau)] - \frac{1}{4}Z_{x\mu\nu}Z_x^{\mu\nu} + \frac{1}{2}m_{Z_x}^2 Z_x^\mu Z_{x\mu}, \end{aligned} \quad (1)$$

where the gauge coupling constant is denoted as g' ; $P_L = \frac{1}{2}(1 - \gamma_5)$ is the left chirality projector; and Q_e , Q_μ , and Q_τ correspond to the charges of leptons of three generations in the $U(1)_{L_e-L_\mu}$ model. The Z_x -field strength tensor can be written as

$$Z_{x\mu\nu} = \partial_\mu Z_{x\nu} - \partial_\nu Z_{x\mu}. \quad (2)$$

Before we discuss the experimental constraints on the gauge boson Z_x , we present the decays of the Z_x boson. The partial decay width of $Z_x \rightarrow \ell^+\ell^- (\nu_\ell\bar{\nu}_\ell)$ for a single flavor lepton is given by

$$\Gamma(Z_x \rightarrow \ell^+\ell^-) = \frac{(g'Q_\ell)^2 M_{Z_x}}{12\pi} \left(1 + \frac{2m_\ell^2}{M_{Z_x}^2}\right) \sqrt{1 - \frac{4m_\ell^2}{M_{Z_x}^2}}, \quad (3)$$

$$\Gamma(Z_x \rightarrow \nu_\ell\bar{\nu}_\ell) = \frac{(g'Q_\ell)^2 M_{Z_x}}{24\pi}. \quad (4)$$

In the $U(1)_{L_e-L_\mu}$ model, the gauge boson Z_x can only couple to two flavor leptons; therefore, the decay channels of the Z_x boson are as follows:

$$Z_x \rightarrow e^+e^-, Z_x \rightarrow \mu^+\mu^-, Z_x \rightarrow \nu_e\bar{\nu}_e, Z_x \rightarrow \nu_\mu\bar{\nu}_\mu. \quad (5)$$

Since $M_{Z_x} \gg M_\ell$, we can neglect the mass of the lepton in Eq. (3), which gives the total width of the gauge boson Z_x as

$$\Gamma_{Z_x} \simeq \frac{g'^2}{4\pi} M_{Z_x}. \quad (6)$$

There are two possible ways to discover the Z_x boson.

On the one hand, the Z_x boson is heavy at the current energy, and we would need a higher energy to find it. On the other hand, it may be that the Z_x mass is very small, and the coupling to the particles in the SM is weak (similar to the search for the Higgs boson); hence, researchers search for it by directly or indirectly producing it at future colliders. In our work, we prefer the latter. When the boson Z_x has a small mass, the τ mass is heavy and unstable, and we mainly consider that the Z_x boson couples only to the e and μ subsets and their corresponding neutrinos in the $U(1)_{L_e-L_\mu}$ model. Some existing constraints on the leptophilic gauge boson mass M_{Z_x} and coupling g' in the $U(1)_{L_e-L_\mu}$ model are summarized in Ref. [26]. The LEP bounds give the most stringent bounds in the larger mass range $M_{Z_x} \leq 10^3$ GeV at $1\sigma(2\sigma)$ via $e^+e^- \rightarrow \ell^+\ell^-$ processes. CMS investigated the final state 4μ for the case that all muons originate from the decay of an (almost) on-shell Z boson, offering good sensitivity for 10 GeV $< M_{Z_x} < 60$ GeV. The strongest constraints on the coupling g' with the 10 – 60 GeV mass range come from the LHC at a 95% confidence level (CL). The g' can be as low as 2×10^{-2} [19, 23]. The production of a muon-antimuon pair in the scattering of muon neutrinos in the Coulomb field of a target nucleus gives a strong bound, e.g., neutrino trident production [27, 28]. A combination

of measurements of the trident cross section from CHARM-II [29], CCFR [30], and NuTeV [31] imposes a bound of $g' \lesssim 1.9 \times 10^{-3} M_{Z_x}/\text{GeV}$ on the $U(1)_{L_e-L_\mu}$ model [23]. The sensitivities from $(g-2)_e$ and $(g-2)_\mu$ on g' in the $U(1)_{L_e-L_\mu}$ model are also considered; their results are in the range $0.2-1$ and $4 \times 10^{-2}-1$, respectively [23, 32–40]. Hence, we propose the process $e^+e^- \rightarrow \ell^+\ell^-Z_x(Z_x \rightarrow \ell^+\ell^-$ or $\nu_\ell\bar{\nu}_\ell)$ in the $U(1)_{L_e-L_\mu}$ model with 10 GeV $\leq M_{Z_x} \leq 60$ GeV to progress further in the search for expected sensitivities of the Z_x boson at the $\sqrt{s} = 240$ GeV CEPC.

III. SEARCHING FOR Z_x AT THE CEPC

The main Feynman diagrams of the signal process $e^+e^- \rightarrow \ell^+\ell^-Z_x(Z_x \rightarrow \ell^+\ell^-$ or $\nu_\ell\bar{\nu}_\ell)$ are shown in Fig. 1, which can be expanded into the following four processes: $e^+e^- \rightarrow e^+e^-Z_x(Z_x \rightarrow e^+e^-) \rightarrow e^+e^-e^+e^-$, $e^+e^- \rightarrow \mu^+\mu^-Z_x(Z_x \rightarrow \mu^+\mu^-) \rightarrow \mu^+\mu^-\mu^+\mu^-$, $e^+e^- \rightarrow e^+e^-Z_x(Z_x \rightarrow \nu_e\bar{\nu}_e) \rightarrow e^+e^-\nu_e\bar{\nu}_e$, and $e^+e^- \rightarrow \mu^+\mu^-Z_x(Z_x \rightarrow \nu_\mu\bar{\nu}_\mu) \rightarrow \mu^+\mu^-\nu_\mu\bar{\nu}_\mu$. In Fig. 2, we present the cross sections of four signaling processes and the corresponding backgrounds. The numerical results for the cross sections are imposed on the basic cuts. We make the transverse momenta of the leptons $P_T(\ell)$ greater than 10 GeV, and the absolute value of the

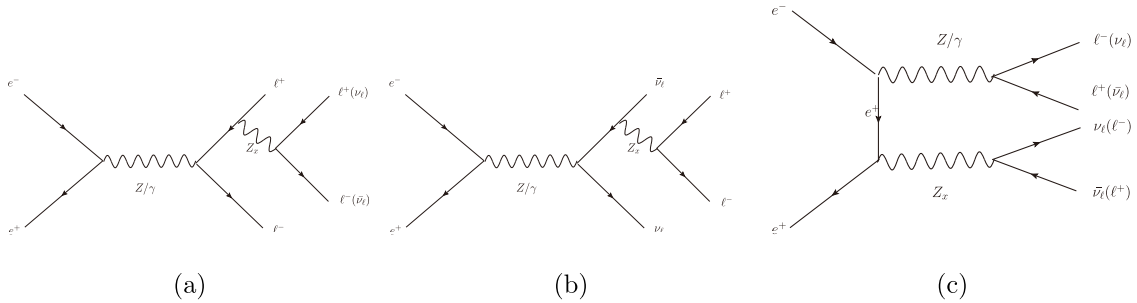


Fig. 1. Main Feynman diagrams for the process $e^+e^- \rightarrow \ell^+\ell^-Z_x(Z_x \rightarrow \ell^+\ell^-$ or $\nu_\ell\bar{\nu}_\ell)$ within $\ell \in \{e, \mu\}$.

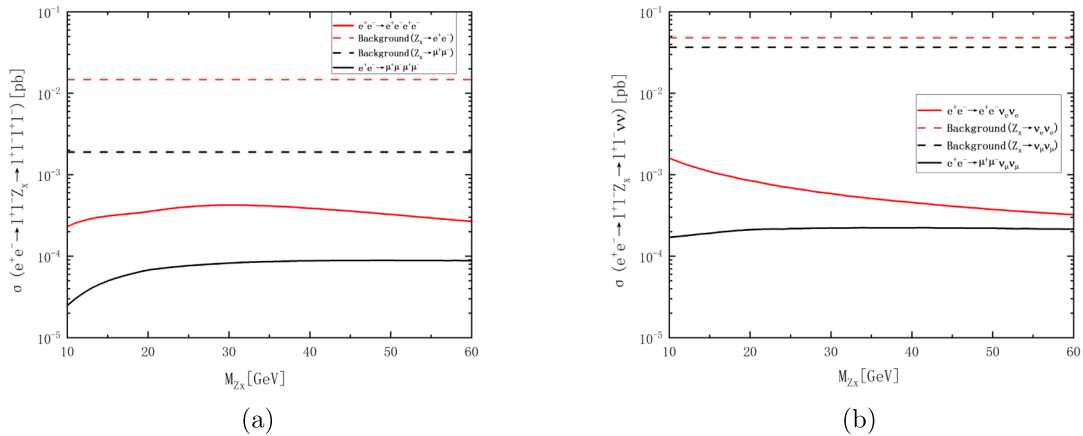


Fig. 2. (color online) Cross sections of the signal and background processes as functions of the mass Z_x when the coupling limits $g' = 0.01$ GeV $^{-1}$.

lepton pseudorapidity η_ℓ needs to be less than 2.5. These basic cuts are then summed up as

$$P_T(\ell) > 10 \text{ GeV}, \quad |\eta_\ell| < 2.5. \quad (7)$$

When the leptophilic gauge boson Z_x decays to a pair of neutrinos, the beam polarizations can help further suppress the SM backgrounds to enhance the signals [41]. Therefore, in the right panel of Fig. 2, we show the polarized cross sections of the $e^+e^- \rightarrow \ell^+\ell^-\nu_\ell\bar{\nu}_\ell$ processes with the beam polarization configurations $(P_{e^+}, P_{e^-}) = (-30\%, +80\%)$. The solid lines represent the signal cross sections, and the dashed lines represent the SM background cross sections. The cross section ranges of signal processes $e^+e^- \rightarrow e^+e^-\nu_e\bar{\nu}_e$ and $e^+e^- \rightarrow \mu^+\mu^-\nu_\mu\bar{\nu}_\mu$ for $10 \text{ GeV} \leq M_{Z_x} \leq 60 \text{ GeV}$ are $3.24 \times 10^{-4} - 1.6 \times 10^{-3} \text{ pb}$ and $1.7 \times 10^{-4} - 2.24 \times 10^{-4} \text{ pb}$, respectively, with $g' = 0.01 \text{ GeV}^{-1}$. For the above two processes, the background cross sections are 0.04823 pb and 0.03663 pb, respectively.

The left panel shows the Z_x boson decaying to a pair of leptons. We consider the effect of polarization on the process $Z_x \rightarrow \ell^+\ell^-$, but the variations in the cross sections are not significant; hence, we do not impose beam polarizations on the cross sections. The solid-red and solid-black lines represent the cross sections of the signal processes $e^+e^- \rightarrow e^+e^-e^+e^-$ and $e^+e^- \rightarrow \mu^+\mu^-\mu^+\mu^-$, respectively. The numerical results are $2.31 \times 10^{-4} - 4.24 \times 10^{-4} \text{ pb}$ and $2.49 \times 10^{-5} - 8.91 \times 10^{-5} \text{ pb}$, respectively, in the mass range $10 \text{ GeV} \leq M_{Z_x} \leq 60 \text{ GeV}$ when the coupling constant $g' = 0.01 \text{ GeV}^{-1}$. The dashed-red and dashed-black lines represent the cross sections of the background processes $e^+e^- \rightarrow e^+e^-e^+e^-$ (0.01477 pb) and $e^+e^- \rightarrow \mu^+\mu^-\mu^+\mu^-$ (0.001899 pb), respectively. The cross sections of signals in the parameter region are smaller than the cross sections of corresponding SM backgrounds.

Next, we used FeynRules [42] to simulate the signals to produce a model file output in the UFO format. Then, all signal and background events were simulated using MadGraph5 [43]; the parton shower and hadronization

were carried out with Pythia8 [44], while the detector simulation was performed using MadAnalysis5 [45] and Delphes3 [46]. In our analysis, we generate, in each case, 10k signal events in an interval where the mass of Z_x increases in order from 10 GeV to 60 GeV, with 500k events for backgrounds.

A. Visible decay channel $Z_x \rightarrow \ell^+\ell^-$

To further improve event selection, the signal and background distributions of the angular separation ΔR between two muons, which is defined as $\Delta R = \sqrt{(\Delta\phi)^2 + (\Delta\eta)^2}$, and invariant masses $M(\mu^+, \mu^-)$ are shown in Fig. 3. We can see that the background and signal have very distinctive characteristics. In particular, for the distribution of invariant masses $M(\mu^+, \mu^-)$, the peaks in $M(\mu^+, \mu^-)$ still denounce the presence of signals, making the distinction against the smooth background easy. We select $M(\mu^+, \mu^-) - M_{Z_x} \leq 5$. ΔR is greater than 0.5 for Z_x mass from 10 GeV to 30 GeV and greater than 0.7 when the Z_x mass is in the mass range 30 – 60 GeV for the process $e^+e^- \rightarrow \mu^+\mu^-\mu^+\mu^-$. Based on the characteristics of the kinematic distributions, the selected cuts are listed in Table 2. After these improved cuts are applied, the SM background is significantly depressed. We take a signal benchmark point every 10 GeV in the 10 – 60 GeV mass interval and display the cross sections of the signal and background after applying the above selection cuts for these benchmark points for $g' = 0.01 \text{ GeV}^{-1}$ at the 240 GeV CEPC with $\mathcal{L} = 5.6 \text{ ab}^{-1}$ in Table 3. We also show the statistical significance (SS) in the last column of Table 3, which is defined as $SS = S / \sqrt{S+B}$, where S represents the number of signal events, and B represents the number of background events. The 1σ , 2σ , 3σ , and 5σ regions in the $g'-M_{Z_x}$ plane are plotted in Fig. 4. The expected bounds on g' can reach 6.2×10^{-3} (8.1×10^{-3}) GeV^{-1} at 3σ (5σ) levels. For the same signal process for the mass $M_{Z_x} < 10 \text{ GeV}$, Ref. [20] provides the upper limit on g' at $SS = 1\sigma$ level; however, we can provide the SS at 3σ (5σ) levels for the mass range 10–60 GeV. Thus, the CEPC has the potential to discover the Z_x boson in

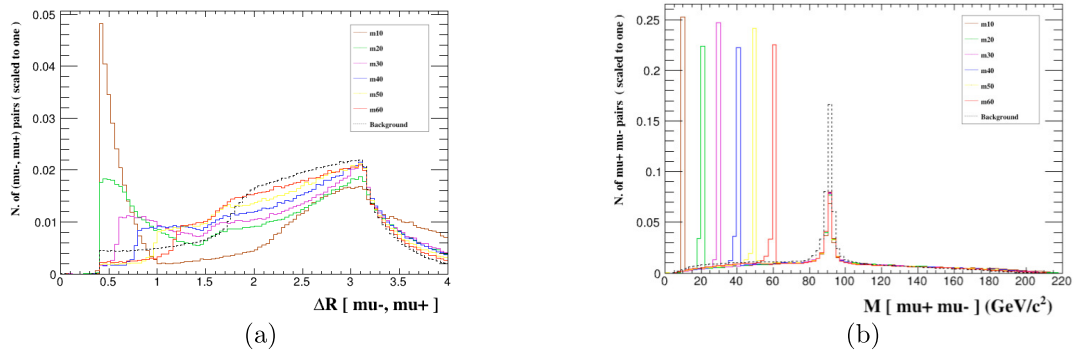


Fig. 3. (color online) Normalized distributions of ΔR (a) and $M(\mu^+, \mu^-)$ (b) from the signal and background events for different M_{Z_x} benchmark points for the process $e^+e^- \rightarrow \mu^+\mu^-\mu^+\mu^-$ at the CEPC with $\sqrt{s} = 240 \text{ GeV}$ and $\mathcal{L} = 5.6 \text{ ab}^{-1}$.

the considered mass range.

For the case where the gauge boson Z_x decays into a pair of electrons, the kinematic distributions of the signal process $e^+e^- \rightarrow e^+e^-e^+e^-$, ΔR , η_{e^-} , η_{e^+} , and $M(e^+, e^-)$ are shown in Fig. 5. The mass of Z_x is greater than 40 GeV, and the distributions of the peaks of η_{e^-} and η_{e^+} are shifted. Therefore, we divide the mass range into two segments of 10–40 GeV and 40–60 GeV when we select the effective cuts. Ultimately, we summarize the specific

Table 2. Improved cuts for the process $e^+e^- \rightarrow \mu^+\mu^-\mu^+\mu^-$.

Cut	Mass	
	$10 \text{ GeV} \leq M_{Z_x} \leq 30 \text{ GeV}$	$30 \text{ GeV} < M_{Z_x} \leq 60 \text{ GeV}$
Cut1	$\Delta R > 0.5$	$\Delta R > 0.7$
Cut2	$M(\mu^+, \mu^-) - M_{Z_x} \leq 5$	$M(\mu^+, \mu^-) - M_{Z_x} \leq 5$

Table 3. Cross sections of the signal and background after imposing the improved cuts for $g' = 0.01 \text{ GeV}^{-1}$ at the CEPC with $\sqrt{s} = 240 \text{ GeV}$ and $\mathcal{L} = 5.6 \text{ ab}^{-1}$ for the process $e^+e^- \rightarrow \mu^+\mu^-\mu^+\mu^-$.

M_{Z_x}/GeV	Cross sections for signal (background)/fb			
	Basic cuts	Cut1	Cut2	SS
10	2.4852×10^{-2} (1.899)	2.4804×10^{-2} (1.894)	2.3443×10^{-2} (0.112)	4.7640
20	6.7516×10^{-2} (1.899)	6.7369×10^{-2} (1.894)	6.3763×10^{-2} (0.346)	7.4520
30	8.2532×10^{-2} (1.899)	8.2393×10^{-2} (1.894)	7.8353×10^{-2} (0.601)	7.1090
40	8.7872×10^{-2} (1.899)	8.7711×10^{-2} (1.894)	8.3870×10^{-2} (0.864)	6.4464
50	8.8983×10^{-2} (1.899)	8.8865×10^{-2} (1.894)	8.5551×10^{-2} (1.109)	5.8548
60	8.8160×10^{-2} (1.899)	8.8096×10^{-2} (1.894)	8.5297×10^{-2} (1.325)	5.3669

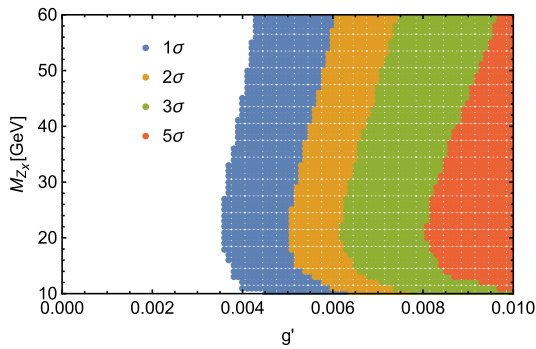


Fig. 4. (color online) 1σ , 2σ , 3σ , and 5σ regions for the process $e^+e^- \rightarrow \mu^+\mu^-\mu^+\mu^-$ at the CEPC with $\sqrt{s} = 240 \text{ GeV}$ and $\mathcal{L} = 5.6 \text{ ab}^{-1}$ in the $g'-M_{Z_x}$ plane.

cuts in Table 4. After applying improved cuts, the cross sections of the signal and the background are shown in Table 5. We also present the regions of SS at 1σ , 2σ , 3σ , and 5σ levels in Fig. 6. As can be seen from the figure, the sensitivity projections of Z_x become weaker with increasing mass, and there is a significant dip at $M_{Z_x} = 30 \text{ GeV}$ with $g' = 5 \times 10^{-3} \text{ GeV}^{-1}$. By comparing the above two processes, the four-electron final state is more sensitive to discovering the Z_x boson.

B. Visible decay channel $Z_x \rightarrow \nu_\ell \bar{\nu}_\ell$

If the Z_x boson decays to a pair of neutrinos, the processes $e^+e^- \rightarrow e^+e^- \nu_e \bar{\nu}_e$ and $e^+e^- \rightarrow \mu^+\mu^- \nu_\mu \bar{\nu}_\mu$ have larger cross sections compared to those for the case when the Z_x boson decays to a pair of leptons. For the process $e^+e^- \rightarrow \mu^+\mu^- \nu_\mu \bar{\nu}_\mu$, according to the kinetic distributions in Fig. 7, the transverse momentum $P_T(\ell)$, invariant mass $M(\mu^+, \mu^-)$, angular separation ΔR between two muons, and transverse energy E_T are improved cuts, as presented in Table 6 for the entire mass range $M_{Z_x} = 10 - 60 \text{ GeV}$. Optimized cuts might preserve as many signal events as

Table 4. Improved cuts for the process $e^+e^- \rightarrow e^+e^-e^+e^-$.

Cut	Mass	
	$10 \text{ GeV} \leq M_{Z_x} \leq 40 \text{ GeV}$	$40 \text{ GeV} < M_{Z_x} \leq 60 \text{ GeV}$
Cut1	$\Delta R > 0.7$	$\Delta R > 1$
Cut2	$\eta_{e^-} > -1.4$	$\eta_{e^-} > -1.1$
Cut3	$\eta_{e^+} < 1.4$	$\eta_{e^+} < 1.1$
Cut4	$M(e^+, e^-) - M_{Z_x} \leq 5$	$M(e^+, e^-) - M_{Z_x} \leq 5$

Table 5. Cross sections of the signal and background after imposing the improved cuts for $g' = 0.01 \text{ GeV}^{-1}$ at the CEPC with $\sqrt{s} = 240 \text{ GeV}$ and $\mathcal{L} = 5.6 \text{ ab}^{-1}$ for the process $e^+e^- \rightarrow e^+e^-e^+e^-$.

M_{Z_x}/GeV	Cross sections for signal (background)/fb					
	Basic cuts	Cut1	Cut2	Cut3	Cut4	SS
10	0.2317 (14.77)	0.2178 (14.18)	0.1965 (12.30)	0.1784 (10.77)	0.1533 (0.9745)	10.7950
20	0.3526 (14.77)	0.3360 (14.18)	0.3124 (12.30)	0.2905 (10.77)	0.2465 (2.602)	10.9270
30	0.4241 (14.77)	0.4061 (14.18)	0.3765 (12.30)	0.3495 (10.77)	0.3027 (4.596)	10.2330
40	0.3876 (14.77)	0.3698 (14.11)	0.3323 (11.27)	0.2984 (9.133)	0.2674 (5.532)	8.3090
50	0.3261 (14.77)	0.3108 (14.11)	0.2839 (11.27)	0.2588 (9.133)	0.2357 (6.696)	6.6985
60	0.2672 (14.77)	0.2544 (14.11)	0.2338 (11.27)	0.2148 (9.133)	0.1984 (7.508)	5.3463

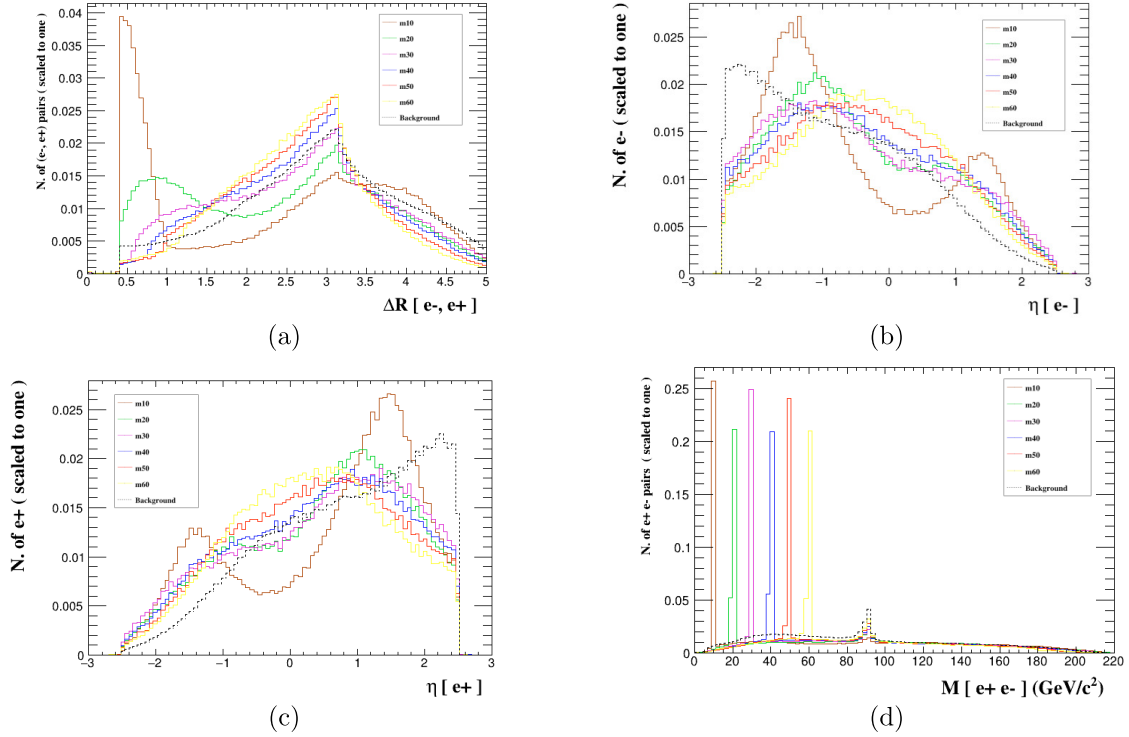


Fig. 5. (color online) Normalized distributions of ΔR (a), η_{e^-} (b), η_{e^+} (c), and $M(e^+, e^-)$ (d) from the signal and background events for different M_{Z_x} benchmark points for the process $e^+e^- \rightarrow e^+e^-e^+e^-$ at the CEPC with $\sqrt{s} = 240$ GeV and $\mathcal{L} = 5.6$ ab^{-1} .

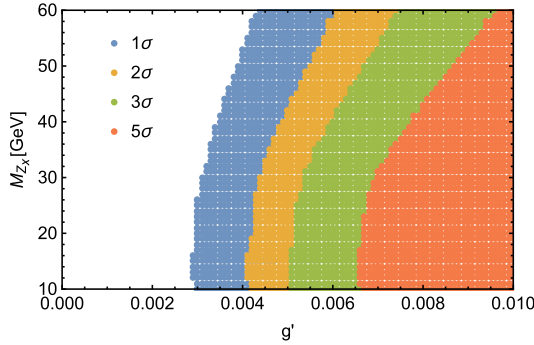


Fig. 6. (color online) 1σ , 2σ , 3σ , and 5σ regions for the process $e^+e^- \rightarrow e^+e^-e^+e^-$ at the CEPC with $\sqrt{s} = 240$ GeV and $\mathcal{L} = 5.6$ ab^{-1} in the g' - M_{Z_x} plane.

possible. Then, we provide the signal and background cross sections after imposing the optimized cuts for the process in Table 7. We can see that, when the background is suppressed by two orders of magnitude, the signal is substantially preserved. Figure 8 shows the $SS = 1\sigma, 2\sigma, 3\sigma, 5\sigma$ ranges in the g' - M_{Z_x} plane; the constraints on the Z_x boson are very strict with the coupling constant g' reaching 6.7×10^{-3} GeV^{-1} at $SS = 5\sigma$.

When Z_x decays to $\nu_e \bar{\nu}_e$, the peak distribution of the e^+ energy for the signal process $e^+e^- \rightarrow e^+e^- \nu_e \bar{\nu}_e$ is clearly demarcated from the background in Fig. 9. For the low mass range $M_{Z_x} = 10 - 40$ GeV, the e^+ energy retains more signals after applying the cuts. On the contrary, for

Table 6. Improved cuts for the process $e^+e^- \rightarrow \mu^+\mu^-\nu_\mu\bar{\nu}_\mu$.

Cut	Mass
	$10 \text{ GeV} \leq M_{Z_x} \leq 60 \text{ GeV}$
Cut1	$P_T(\ell) > 5$
Cut2	$ M(\mu^+, \mu^-) - M_{Z_x} \leq 5$
Cut3	$\Delta R < 4$
Cut4	$E_T < 150$

the large mass range $M_{Z_x} = 40 - 60$ GeV, the signal events of the invariant mass $M(e^+, e^-)$ outnumber the signal events of $E(e^+)$ after improving cuts; therefore, we add to the effective cuts at $M_{Z_x} = 40$ GeV, as shown in Table 8. Finally, Table 9 presents the cross sections of the signal and background after the improved cuts are imposed on the $e^+e^- \rightarrow e^+e^- \nu_e \bar{\nu}_e$ process, and we plot $1\sigma, 2\sigma, 3\sigma$ and 5σ ranges in Fig. 10. The sensitivity projections of the Z_x boson that we obtain are very strict for the process, especially in the region of mass $M_{Z_x} = 10 - 40$ GeV. In contrast to the three processes mentioned above, this process is more sensitive to the Z_x boson.

IV. CONCLUSION AND DISCUSSION

Recently, there have been many studies related to the leptophilic gauge boson Z_x . The search for the mass range of $10 - 500$ GeV Z_x in the $U(1)_{L_\mu - L_\tau}$ model is widely stud-

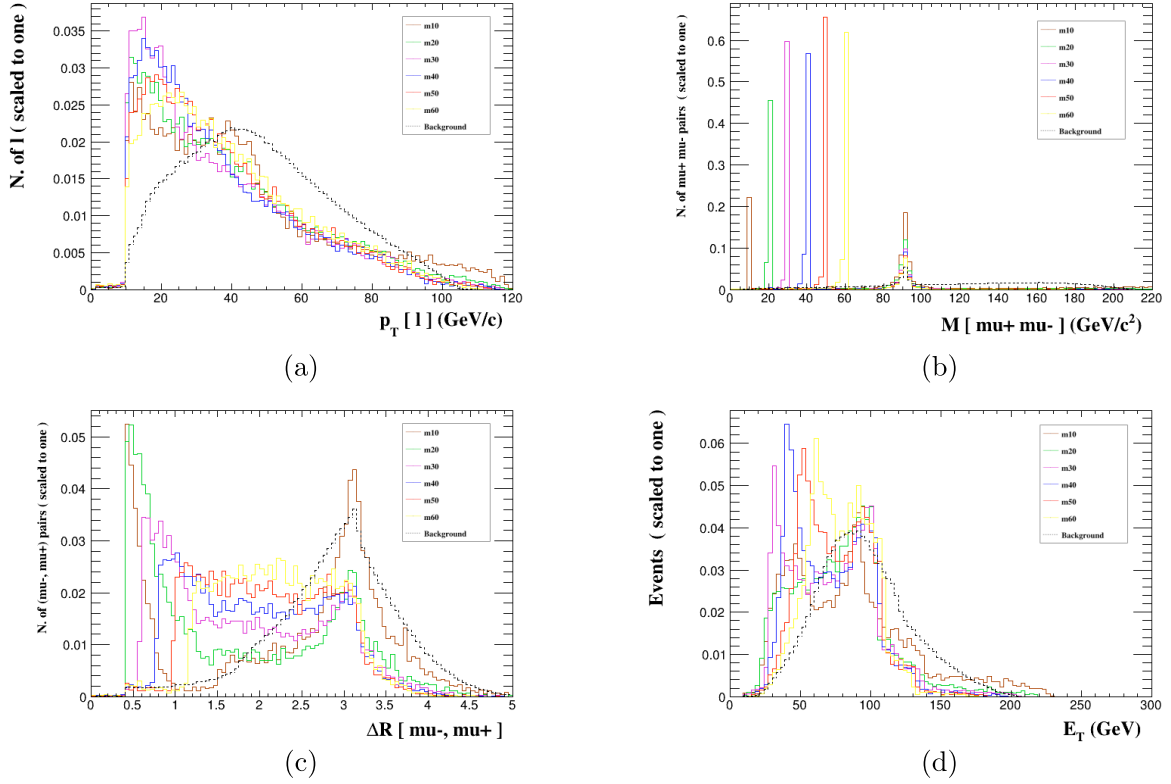


Fig. 7. (color online) Normalized distributions of $P_T(\ell)$ (a), $M(e^+e^-)$ (b), ΔR (c), and E_T (d) from the signal and background events for different M_{Z_x} benchmark points for the process $e^+e^- \rightarrow \mu^+\mu^-\nu_\mu\bar{\nu}_\mu$ at the CEPC with $\sqrt{s} = 240$ GeV and $\mathcal{L} = 5.6$ ab^{-1} .

Table 7. Cross sections of the signal and background after imposing the improved cuts for $g' = 0.01$ GeV^{-1} at the CEPC with $\sqrt{s} = 240$ GeV and $\mathcal{L} = 5.6$ ab^{-1} for the process $e^+e^- \rightarrow \mu^+\mu^-\nu_\mu\bar{\nu}_\mu$.

M_{Z_x}/GeV	Cross sections for signal (background)/fb					
	Basic cuts	Cut1	Cut2	Cut3	Cut4	SS
10	0.1708 (36.63)	0.1706 (36.59)	0.03665 (0.2205)	0.03665 (0.2205)	0.03665 (0.2200)	5.4300
20	0.2122 (36.63)	0.2215 (36.59)	0.1054 (0.4993)	0.1054 (0.4993)	0.1054 (0.4985)	10.1420
30	0.2216 (36.63)	0.2215 (36.59)	0.1317 (0.6723)	0.1317 (0.6721)	0.1317 (0.6711)	11.0030
40	0.2229 (36.63)	0.2215 (36.59)	0.1317 (0.8064)	0.1317 (0.8056)	0.1414 (0.8046)	10.8980
50	0.2205 (36.63)	0.2204 (36.59)	0.1467 (0.9205)	0.1467 (0.9195)	0.1467 (0.9195)	10.5890
60	0.2153 (36.63)	0.2153 (36.59)	0.1443 (1.037)	0.1443 (1.036)	0.1443 (1.034)	9.9480

ied at the LHC. However, the search for a small mass of Z_x is very limited in the $U(1)_{L_e-L_\mu}$ model at the future e^+e^- colliders. It is evident that there is still a large para-

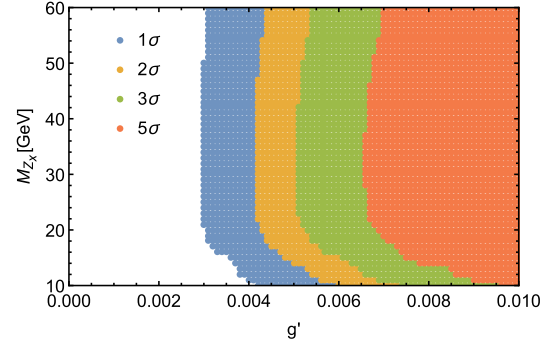


Fig. 8. (color online) 1σ , 2σ , 3σ and 5σ regions for the process $e^+e^- \rightarrow \mu^+\mu^-\nu_\mu\bar{\nu}_\mu$ at the CEPC with $\sqrt{s} = 240$ GeV and $\mathcal{L} = 5.6$ ab^{-1} in the $g'-M_{Z_x}$ plane.

meter space around the electroweak scale for us to explore the Z_x boson [23]. Thus, we can search for the Z_x predicted by the $U(1)_{L_e-L_\mu}$ model at the CEPC to facilitate the extension of the sensitivity of Z_x or stricter couplings. In our study, we investigate the prospects of the CEPC to unravel the NP associated with a new weak interaction, and the gauge boson Z_x only couples to the e and μ subsets in the $U(1)_{L_e-L_\mu}$ model.

We investigated the sensitivity of the CEPC with $\sqrt{s} = 240$ GeV and $\mathcal{L} = 5.6$ ab^{-1} to the coupling parameter g' for $M_{Z_x} = 10-60$ GeV. As can be seen from the four

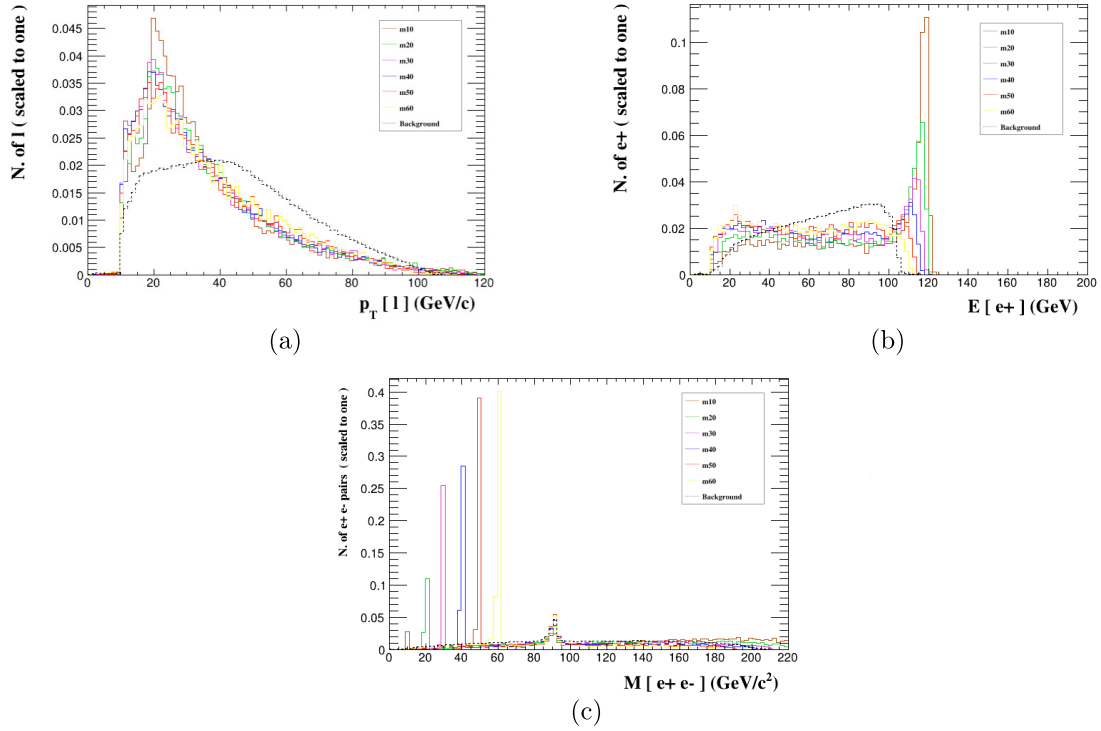


Fig. 9. (color online) Normalized distributions of $P_T(\ell)$ (a), $E(e^+)$ (b), and $M(e^+, e^-)$ (c) from the signal and background events for different M_{Z_x} benchmark points for the process $e^+e^- \rightarrow e^+e^- \nu_e \bar{\nu}_e$ at the CEPC with $\sqrt{s} = 240$ GeV and $\mathcal{L} = 5.6$ ab^{-1} .

Table 8. The improved cuts for the process $e^+e^- \rightarrow e^+e^- \nu_e \bar{\nu}_e$.

Cut	Mass	
	$10 \text{ GeV} \leq M_{Z_x} \leq 40 \text{ GeV}$	$40 \text{ GeV} < M_{Z_x} \leq 60 \text{ GeV}$
Cut1	$P_T(\ell) > 5$	$P_T(\ell) > 5$
Cut2	$E(e^+) > 110$	$ M(e^+, e^-) - M_{Z_x} \leq 5$

processes explored in the previous sections, the expected bounds of the process $e^+e^- \rightarrow e^+e^- \nu_e \bar{\nu}_e$ on g' can reach 1.0×10^{-3} (1.6×10^{-3}) GeV^{-1} for $M_{Z_x} = 10 - 40$ GeV at 3σ (5σ); these are the strictest constraints on the $U(1)_{L_e-L_\mu}$ model. However, in the Z_x mass range of 40–60 GeV, the strictest constraints come from the process $e^+e^- \rightarrow \mu^+\mu^- \nu_\mu \bar{\nu}_\mu$, and the expected bounds on g' can reach 5.1×10^{-3} (6.7×10^{-3}) GeV^{-1} at 3σ (5σ). Compared to the other three processes, the process $e^+e^- \rightarrow \mu^+\mu^- \mu^+\mu^-$ is less constrained.

In conclusion, the expected sensitivities of the four processes to the parameter space of the $U(1)_{L_e-L_\mu}$ models are different. However, when we compare our numerical results in Fig. 2 with those in Ref. [23], they are not experimentally excluded except from the process $e^+e^- \rightarrow \mu^+\mu^- \mu^+\mu^-$. At the same time, Ref. [24] indicates that the sensitivity to g' for the process $e^+e^- \rightarrow Z_x \gamma$ can be as low as 5×10^{-3} in the mass range of 10–60 GeV at the 2σ level. Our results can reach 1×10^{-3} for $M_{Z_x} = 10$ GeV via the process $e^+e^- \rightarrow e^+e^- \nu_e \bar{\nu}_e$, and the constraints from the

Table 9. Cross sections of the signal and background after imposing the improved cuts for $g' = 0.01$ GeV^{-1} at the CEPC with $\sqrt{s} = 240$ GeV and $\mathcal{L} = 5.6$ ab^{-1} for the process $e^+e^- \rightarrow e^+e^- \nu_e \bar{\nu}_e$.

M_{Z_x}/GeV	Cross sections for signal (background)/fb			
	Basic cuts	Cut1	Cut2	SS
10	1.6011 (48.23)	1.5658 (46.75)	0.49924 (0.02334)	51.6830
20	0.8491 (48.23)	0.8312 (46.75)	0.1709 (0.02334)	28.9830
30	0.5879 (48.23)	0.5761 (46.75)	0.06803 (0.02334)	16.7940
40	0.4583 (48.23)	0.4491 (46.75)	0.02810 (0.02334)	9.2220
50	0.3755 (48.233)	0.3677 (46.75)	0.1192 (1.522)	7.3630
60	0.3247 (48.23)	0.3172 (46.75)	0.1187 (0.1187)	6.6180

process $e^+e^- \rightarrow \mu^+\mu^- \nu_\mu \bar{\nu}_\mu$ can reach 4.2×10^{-3} at the 2σ level in the entire mass range of 10–60 GeV. Our numerical results align with those of Ref. [24], as the same conclusions are applicable to the process $e^+e^- \rightarrow e^+e^- e^+e^-$. Hence, searching for the Z_x boson predicted by the

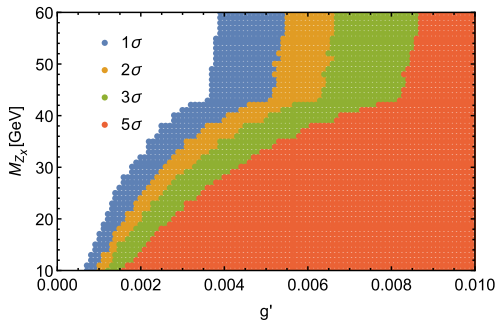


Fig. 10. (color online) 1σ , 2σ , 3σ , and 5σ regions for the process $e^+e^- \rightarrow e^+e^-\nu_e\bar{\nu}_e$ at the CEPC with $\sqrt{s} = 240$ GeV and $\mathcal{L} = 5.6 \text{ ab}^{-1}$ in the $g'-M_{Z_x}$ plane.

$U(1)_{L_e-L_\mu}$ model at the 240 GeV CEPC via processes $e^+e^- \rightarrow \ell^+\ell^-Z_x(Z_x \rightarrow \nu_\ell\bar{\nu}_\ell$ or $\ell\ell)$ can enhance the sensitivity projections to the parameter space and promote further exploration of future e^+e^- colliders for the $U(1)_{L_e-L_\mu}$ model, providing more opportunities for further discoveries regarding the leptophilic gauge boson Z_x .

ACKNOWLEDGEMENTS

Yan-Yu Li would like to thank Han Wang for very useful discussions.

References

- [1] M. Dong *et al.* (CEPC Study Group) (2018), arXiv: [1811.10545](#)
- [2] R. Foot, *Mod. Phys. Lett. A* **6**, 527 (1991)
- [3] X.-G. He, G. C. Joshi, H. Lew *et al.*, *Phys. Rev. D* **44**, 2118 (1991)
- [4] R. Foot, X. G. He, H. Lew *et al.*, *Phys. Rev. D* **50**, 4571 (1994), arXiv:[hepph/9401250](#)
- [5] W. Buchmuller, C. Greub, and P. Minkowski, *Phys. Lett. B* **267**, 395 (1991)
- [6] R. E. Marshak and R. N. Mohapatra, *Phys. Lett. B* **91**, 222 (1980)
- [7] S. Baek, H. Okada, and K. Yagyu, *JHEP* **04**, 049 (2015), arXiv:[1501.01530](#)
- [8] J. Heeck and W. Rodejohann, *Phys. Rev. D* **84**, 075007 (2011), arXiv:[1107.5238](#)
- [9] A. Biswas, S. Choubey, and S. Khan, *JHEP* **09**, 147 (2016)
- [10] S. Patra, S. Rao, N. Sahoo *et al.*, *Nucl. Phys. B* **917**, 317 (2017), arXiv:[1607.04046](#)
- [11] G. Arcadi, T. Hugle, and F. S. Queiroz, *Phys. Lett. B* **784**, 151 (2018), arXiv:[1803.05723](#)
- [12] W. Altmannshofer, S. Gori, S. Profumo *et al.*, *JHEP* **12**, 106 (2016), arXiv:[1609.04026](#)
- [13] S. N. Gninenko and N. V. Krasnikov, *Phys. Lett. B* **513**, 119 (2001), arXiv:[hep-ph/0102222](#)
- [14] E. Ma, D. P. Roy, and S. Roy, *Phys. Lett. B* **525**, 101 (2002), arXiv:[hep-ph/0110146](#)
- [15] S. Baek, N. G. Deshpande, X. G. He *et al.*, *Phys. Rev. D* **64**, 055006 (2001), arXiv:[hepph/0104141](#)
- [16] A. D. Medina, N. I. Mileo, A. Szykman *et al.*, *Phys. Rev. D* **106**, 075018 (2022), arXiv:[2112.09103](#)
- [17] A. M. Sirunyan *et al.* (CMS), *Eur. Phys. J. C* **78**, 165 (2018) [Erratum: *Eur. Phys. J. C* **78**, 515 (2018)], arXiv: [1709.08601](#)
- [18] A. M. Sirunyan *et al.* (CMS), *JHEP* **03**, 166 (2018)
- [19] M. Drees, M. Shi, and Z. Zhang, *Phys. Lett. B* **791**, 130 (2019), arXiv:[1811.12446](#)
- [20] T. Czank *et al.* (Belle), *Phys. Rev. D* **106**, 012003 (2022)
- [21] S. Schael *et al.* (ALEPH, DELPHI, L3, OPAL, LEP Electroweak), *Phys. Rept.* **532**, 119 (2013)
- [22] J. P. Lees *et al.* (BaBar), *Phys. Rev. Lett.* **113**, 201801 (2014), arXiv:[1406.2980](#)
- [23] A. Dasgupta, P. S. B. Dev, T. Han *et al.*, (2023), arXiv: [2308.12804](#)
- [24] M. He, X.-G. He, C.-K. Huang *et al.*, *JHEP* **03**, 139 (2018), arXiv:[1712.09095](#)
- [25] Z. Liu, Y.-H. Xu, and Y. Zhang, *JHEP* **06**, 009 (2019), arXiv:[1903.12114](#)
- [26] E. J. Chun, A. Das, J. Kim *et al.*, *JHEP* **02**, 093 (2019) [Erratum: *JHEP* **07**, 024 (2019)], arXiv: [1811.04320](#)
- [27] W. Altmannshofer, S. Gori, M. Pospelov *et al.*, *Phys. Rev. Lett.* **113**, 091801 (2014), arXiv:[1406.2332](#)
- [28] R. Belusevic and J. Smith, *Phys. Rev. D* **37**, 2419 (1988)
- [29] D. Geiregat *et al.* (CHARM-II), *Phys. Lett. B* **245**, 271 (1990)
- [30] S. R. Mishra *et al.* (CCFR), *Phys. Rev. Lett.* **66**, 3117 (1991)
- [31] T. Adams *et al.* (NuTeV), in *29th International Conference on High-Energy Physics* (1998), pp. 631-634, arXiv: [hep-ex/9811012](#)
- [32] M. Pospelov, *Phys. Rev. D* **80**, 095002 (2009), arXiv:[0811.1030](#)
- [33] M. Laine, L. Niemi, S. Procacci *et al.*, *JHEP* **11**, 126 (2022)
- [34] T. Aoyama, T. Kinoshita, and M. Nio, *Atoms* **7**, 28 (2019)
- [35] L. Morel, Z. Yao, P. Cladé *et al.*, *Nature* **588**, 61 (2020)
- [36] R. H. Parker, C. Yu, W. Zhong *et al.*, *Science* **360**, 191 (2018), arXiv:[1812.04130](#)
- [37] B. Abi *et al.* (Muon g-2), *Phys. Rev. Lett.* **126**, 141801 (2021), arXiv:[2104.03281](#)
- [38] D. P. Aguillard *et al.* (Muon g-2), *Phys. Rev. Lett.* **131**, 161802 (2023), arXiv:[2308.06230](#)
- [39] G. W. Bennett *et al.* (Muon g-2), *Phys. Rev. D* **73**, 072003 (2006), arXiv:[hep-ex/0602035](#)
- [40] T. Aoyama *et al.*, *Phys. Rept.* **887**, 1 (2020), arXiv:[2006.04822](#)
- [41] S.-F. Ge, K. Ma, X.-D. Ma *et al.*, (2023), arXiv: [2306.00657](#)
- [42] A. Alloul, N. D. Christensen, C. Degrande *et al.*, *Comput. Phys. Commun.* **185**, 2250 (2014), arXiv:[1310.1921](#)
- [43] J. Alwall, R. Frederix, S. Frixione *et al.*, *JHEP* **07**, 079 (2014), arXiv:[1405.0301](#)
- [44] T. Sjostrand, S. Mrenna, and P. Z. Skands, *Comput. Phys. Commun.* **178**, 852 (2008), arXiv:[0710.3820](#)
- [45] E. Conte, B. Fuks, and G. Serret, *Comput. Phys. Commun.* **184**, 222 (2013), arXiv:[1206.1599](#)
- [46] J. de Favereau *et al.* (DELPHES 3), *JHEP* **02**, 057 (2014), arXiv: [1307.6346](#)